MODESTUM
OPEN ACCESS

Eurasian Journal of Analytical Chemistry, 2018, 13(5), em64
ISSN:1306-3057
Research Paper https://doi.org/10.29333/ejac/97267

Synthesis, Spectral and Biological Studies of Ni(II), Pd(II), and Pt(IV) Complexes with New Heterocyclic ligand Derived from Azo-Schiff Bases Dye

Khalid J. Al-Adilee [1*], Haitham K. Dakheel [1]

[1] Department of Chemistry, College of Education, University of Al-Qadisiyah, Diwaniya 1753, IRAQ

Received 23 May 2018 ▪ Revised 12 September 2018 ▪ Accepted 22 September 2018

ABSTRACT

New heterocyclic azo-schiff base dye (L_2) have been synthesized from a reaction of 4-(dimethylamino)benzaldehyde with (E)-5-((1H-benzo[d]imidazol-2-yl) diazenyl) -2-amine-4,6-dimethylpyridin (L_1) . A new class of Ni(II), Pd(II), and Pt(IV) complexes of azo- schiff base of the type $[Ni(L_2)_2Cl_2]$, $[Pd(L_2)\ Cl_2]$, and $[Pt(L_2)_2Cl_2]Cl_2$ where L_2=(E)-5-((E)-(1H-benzo[d]imidazol-2-yl)diazenyl)-N-(4-(dimethylamino)benzylidene) -2-amine- 4,6-dimethylpyridin. Both ligand and its metal complexes were characterized by the spectroscopic and analytical methods such as mass spectral, ^{1}H- NMR, FT- IR, UV-Visb.,X- ray, TGA and SEM, elemental analysis, molar conductance measurements and magnetic susceptibility., spectral studies suggest the mole ratio [M:L] was [1:2] for Ni(II) and Pt(IV) metal ions, but [1:1] for Pd(II) metal ion. The structures of theses complexes were elucidated on the basis of different techniques suggest the structures of the prepared metal complexes octahedral geometry for the Ni(II) and Pt(IV) complexes and square planar geometry for the Pd(II) complex. The antibacterial activity of the ligand and prepared metal complexes was also studied against gram positive *Staphylococcus aureus* and gram negative bacteria *Escherichia coli*, the antifungal activity of the azo-schiff base and metal complexes against the *fungi Alternaria*. It is found that some of the complexes are quite effective against *fungi Alternaria*. In this study the cytotoxicity of Pd(II)-complex on human (PC3) cancer and normal cells were studied using MTT assay. Pd(II)-complex showed selective cytotoxicity against cancer cell line with IC_{50} = 450 µg/ml, while it was very safe on normal cells line with IC_{50} = 14554885 µg /ml, respectively for human cells .The results indicate undoubtedly the possibility of using them as antitumor drugs in the field of medicine and Pharmacy against prostate cancer.

Keywords: synthesis, azo-schiff base, metal complexes, X- ray diffraction, TGA and SEM, spectral studies, antibacterial, antifungal and anticancerious

INTRODUCTION

Azo-schiff dyes derivatives are important class of organic complexing compounds. This compound is more activity and less toxic antimicrobial agents result to the increase in resistance to the available antimicrobial drugs [1]. Azo-schiff base compounds are famous for exhibit the wide range of applications in antimicrobial, pharmaceutical, industrial and analytical reagents uses [2,3]. These compounds are also a kind of multipurpose ligands in coordination chemistry [4-6]. Also transition metal complexes of azo schiff bases are found to be useful as anticancer agents, antibacterial [7-10], as excellent homogeneous and heterogeneous-phase catalysts [11], and as chemical sensors [12]. Cancer, known as the malignant tumor or malignant neoplasm, is the kind of diseases characterized by out-of-control cell growth [13]. Around a world, big number of people are diagnosed with cancer each year, and most of a patients die from it [14]. Several strategies are being developed to fight against cancer [15-17]. Cis- Pt(II) complex is the first number of platinum-containing anti-cancer drug [18]. Despite greatly effective in treating the

✉ khalid.jawad@qu.edu.iq **(*Correspondence)**

various types of cancers, cis-Pt(II) complex has the number of side-effects such as nephrotoxicity, neurotoxicity and ototoxicity *etc* [19,20]. Side-effect problems of cis–Pt(II) have stimulated chemists to develop alternative anticancer drugs based on different metals. Several studies indicated that copper complexes had showed some promising results [21]. In this study we report the synthesis, spectra characterization of azo –schiff base ligand and its metal complexes with Ni(II), Pd(II), and Pt(IV) ions derived from (E)-5-((E)-(1H-benzo[d]imidazol-2-yl)diazenyl)-N-(4-(dimethylamino)benzylidene) -2-amine -4,6-dimethylpyridin (L_2). The antibacterial activity of the prepared complexes was also studied against gram positive *Staphylococcus aureus* and gram negative bacteria *Escherichia coli and* antifungal activity of the azo-schiff base and metal complexes against the *fungi Alternaria*. Also in this study the cytotoxicity of Pd(II)-complex on human (PC3) cancer and normal cells were studied using MTT assay.

EXPERIMENTAL

Materials and Measurements

All chemicals and solvents used in the present work were high purity provided from multiple companies such as Fluk, BDH, Aldrich and Sigma and used without further purification. Doubly distilled water was used in all experiments. Elemental analysis of azo-schiff base dyes. Ligand and its metal complexes were carried out by mean of micro analytical unit of EA 300 C.H.N Element analyzer. Mass spectra were obtained using a shimadzu Agilent Technologies 5973C at 70^e and MSD energy using a direct insertion probe (Acq method 10 W energy) at temperature 90-110 °C. ^{1}H**-** NMR spectra were recorded on a model Bruker 500 MHZ spectro photometer using DMSO-d_6 as a solvent and TMS as an internal standard. Electronic spectra were measured in absolute ethanol as a solvent (10^{-3}M) in the range (200-1100) nm by using a UV-Visb. T80-PG spectrophotometer. Infrared spectra were recorded in KBr medium as dics using a shimadzu 8400S FT-IR spectrophotometer in wave number at range (4000-400) cm^{-1} .X-ray diffraction were measured using Bestec Germany Aluminum anode model X pertpro, wavelength of X-ray beam(Cu k_α) 1.54 angstrom, Anod material=Cu, the Voltage = 40KV and current = 30mA. The magnetic susceptibility for the prepared metal complexes were measured at room temperature using faraday method. For this purpose, Burker Magnet (B.M) had been employed and the diamagnetic correction were made by pascals constants. TGA, DSC and DTG analysis were measured with England PL- TG using Rheometric scientific TGA-1000. SEM images of ligand and Pd (II)-complex, were taken using micrograph kyky 3200. Electric molar conductivity measurements were carried out at room temperature in DMF (10^{-3} M) solution by using conductivity bridge model 31A. The melting points of ligand (L_2) and its complexes were measured by using electro thermal melting point 9300. The pH solutions were measured on a PW 9421 pH meter (±0.001). The chloride ion content in Pt(IV)-complex was determined by more.

Synthesis of Azo-Schiff Base Ligand (L_2)

Azo-schiff base ligand (L_2) was synthesized following the analogous procedure Al-Adilee *etal* [22,23] with some modification in a two-step process as described below. In the first step, 2-Amino benzimidazole (0.133 gm, 1mmoc) was dissolved in mixture of 3 ml concentrated hydrochloric acid and 30 mL distilled water with continuously (**Scheme 1**) cooing and stirring until reach the temperature (0-5) °C and diazotized below 5 °C with solution of sodium nitrite $NaNO_2$ (0.75 gm,1 mmol, dissolved in 20 ml distilled water) was added in drops. The diazonium chloride compound was then coupled with 2-amine-4,6-dimethylpyridin in alkaline media below 5 °C. The pH value during the coupling was maintained between 6-7, coupling to the 2-amine-4,6-dimethylpyridin occurred in basic media at the *para*-position to the amine group. (E)-5-((1H-benzo[d]imidazol-2-yl) diazenyl) -2-amine -4,6-dimethylpyridin (L_1) in the second step, the ligand (L_2) was synthesized according to the known condensation method. About (0.266 g, 1 mmol) of (L_1) in absolute ethanol (20 ml) was added drop-wise to hot absolute ethanol (50 ml) solution of 4-(dimethylamino)benzaldehyde (0.149 g, 1 mmol) with few drops of glacial acetic acid as a catalyst (**Scheme 1**). The mixture was refluxed and stirred continuously for 3 h at 80 °C. After cooling, the solid product was filtered off, and washed several times with cold distilled water then dried in vacuum for several hours and recrystallized twice from hot ethanol to afford red crystals coloured product and stored in a desiccator over anhydrous calcium chloride. Yield: 76%; m.p. 152 °C The purity was confirmed by the elemental analysis and thin layer chromatography TLC techniques. The structure of azo schiff base ligand (L_2) was clucidated by 'H-NMR, mass spectrum, IR and UV-visb. spectra. The structural of the ligand (L_2) as shown in **Scheme 1**.

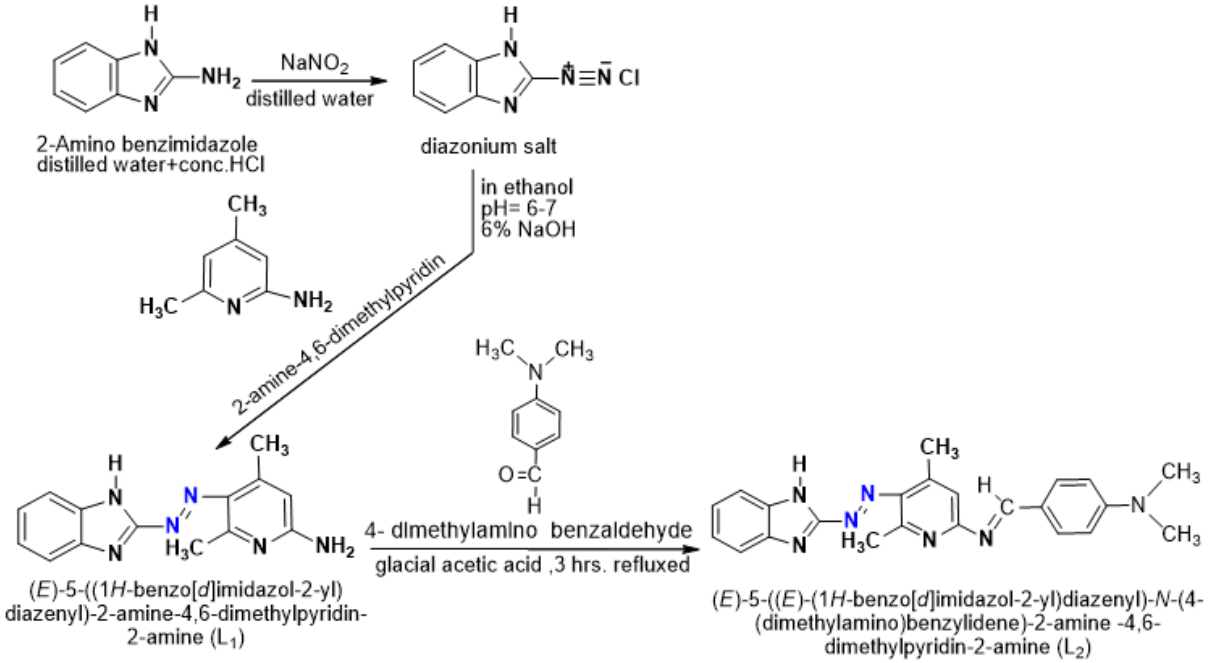

Scheme 1. Preparation of new azo-schiffbaes ligand (L_2)

Table 1. Analytical and physical data of ligand (L_2) and its metal complexes

compound	color	m.p °C	Yield%	Molecular Formula (Mol.wt)	Found (calc.)%			
					C	H	N	M
Ligand =I_2	Light red	152	76	$C_{23}H_{23}N_7$ (397.47)	(69.50) 70.01	(5.83) 5.91	(24.67) 24.99	---------
$[Ni(L_2)_2Cl_2].H_2O$	purple	189	68	$C_{46}H_{48}Cl_2N_{14}NiO$ (942.57)	(58.62) 58.83	(5.13) 5.19	(20.80) 21.08	(6.23) 6.42
$[Pd(L_2)\ Cl_2]$	brown	178	61	$C_{23}H_{23}Cl_2N_7Pd$	(48.06) 48.37	(4.03) 4.15	(17.06) 17.35	(18.51) 19.13
$[Pt(L_2)_2Cl_2]Cl_2$	greenish blue	204	83	$C_{46}H_{46}Cl_4N_{14}Pt$ ((1131.84	(48.81) 49.27	(4.10) 4.18	(17.33) 17.64	(17.24) 17.51

Synthesis of Metal Complexes

The Ni(II)-complex was prepared by dissolving (0.397 gm , 1 mmol) from azo-schiff base ligand (L_2) in hot ethanol than added in drops with stirring continuously to (1 mmol), 1:2 [M;L], for Ni(II) chloride salt dissolved in 20 ml hot buffer solution (ammonium acetate) at PH=7.0, the resulting solutions were refluxed for 1 hour and then the volume of the solution was reduced to one-half by evaporation. The obtained solution was left for 1 hour in the freezer; compounds were filtered off, washed with absolute ethanol and recrystallized in ethanol [24-26].

The Pd(II) and Pt(IV) -complexes were prepared by dissolving (0.397 gm , 1 mmol) from azo-schiff base ligand (L_2) in hot methanol than added 20 ml methanolic solution of Pd(II) and Pt(IV) chloride salt (Pd(II) chloride salt 1 mmol, but Pt(IV) chloride salt 0.5 mmol) and refluxed for 1 hour. The precipitate was filtered off, washed with distilled water and washed with 5 ml methanol to remove any traces of unreacted materials and dried in air [27-29]. The % yield, m.p, pH, color, molecular formula, M.wt and element analysis data (C.H.N) of ligand and its metal complexes are collected in **Table 1**.

RESULT AND DISCUSSION

Characterization of Azo Schiff Base Ligand (L2) and its Metal Complexes

The metal complexes derived from azo -schiff base ligand (L_2) are stable toward air and insoluble in water and some common organic solvents but soluble in ethanol, methanol, dimethylformamide, dimethylsulfoxide and acetone. The physical characteristics and microanalytical data of the ligand (L_2) and their metal complexes are given in experimental section. The structures of the obtained ligand and their respective metal complexes were clucidated

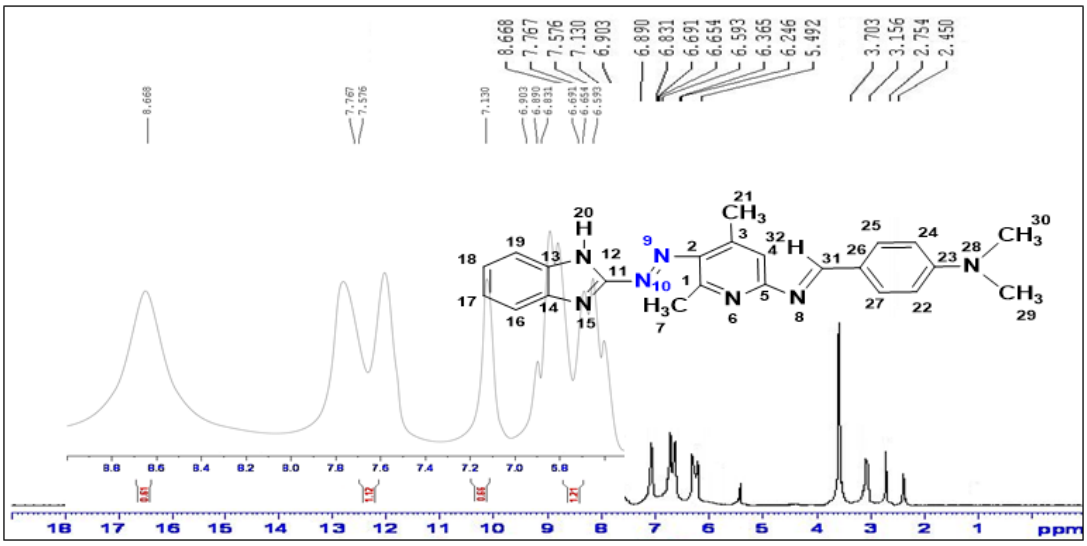

Figure 1. ^{1}H-NMR spectrum of azo – cshiff base ligand (L_2)

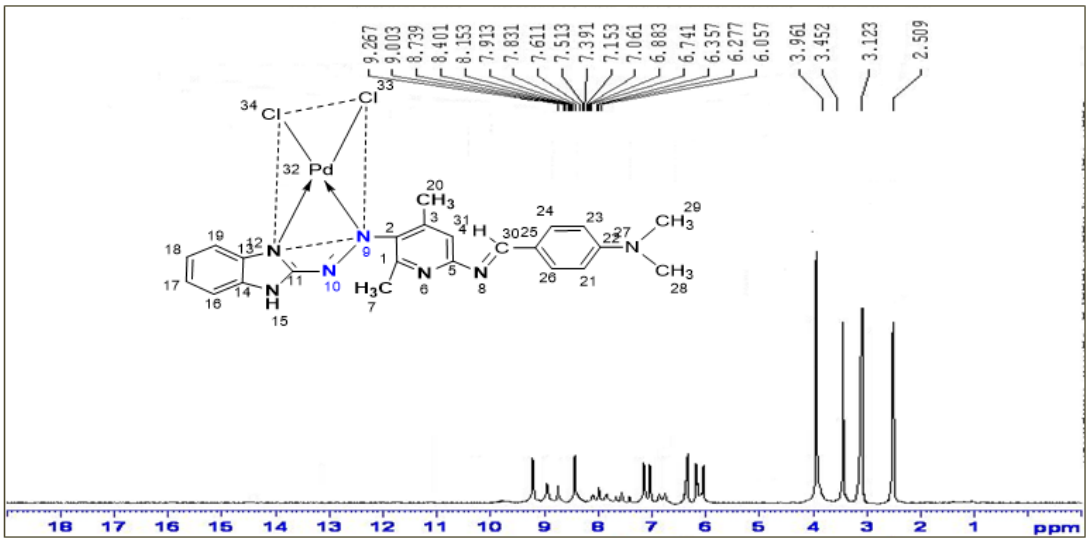

Figure 2. ^{1}H-NMR spectrum of Pd(II)- complex

by, infrared, elemental analysis, mass spectra, ^{1}H-NMR, UV–visib spectra and several techniques. Microanalytical data for the ligand (L_2) and its metal complexes are in very good agreement with theoretical values.

^{1}H-NMR Spectra

The ^{1}H- NMR spectral results, obtained for Azo-schiff base ligands (L_2) and Pd(II) complex at ambient temperature in DMSO-d_6, with TMS as an internal reference is assigned as follows: the characteristic singlet at δ= 8.668 ppm is due to the azomethine proton (–CH=N), and multiplets around δ = 6.246-7.767 ppm are assigned to aromatic protons and three signal at δ =2.745,3.156,3.703 ppm is ascribed to methyl group. A singlet at δ=5.492 ppm is attributed to the (NH) group in imidazole ring of the Azo-schiff base. A signal at δ =2.450 ppm assigned to solvent proton [30-32].

The ^{1}H-NMR spectrum of pd(II)-complex shows change in a signal at δ = 6.857 ppm (imidazole proton) due to the presence of NH group in the spectrum of the pd(II)-complex is shifted down field compared to the free ligand, suggesting deshielding of the amine group due to the coordination with metal ion singlet at δ =9.267 ppm is due to the azomethine proton (–CH=N), and multiplets around δ = 6.557-9.003 ppm are assigned to aromatic protons and three signal at δ = 3.123,3.452 and 3.961 ppm is ascribed to methyl group. A signal at δ =2.509 ppm assigned to solvent proton [33,34].

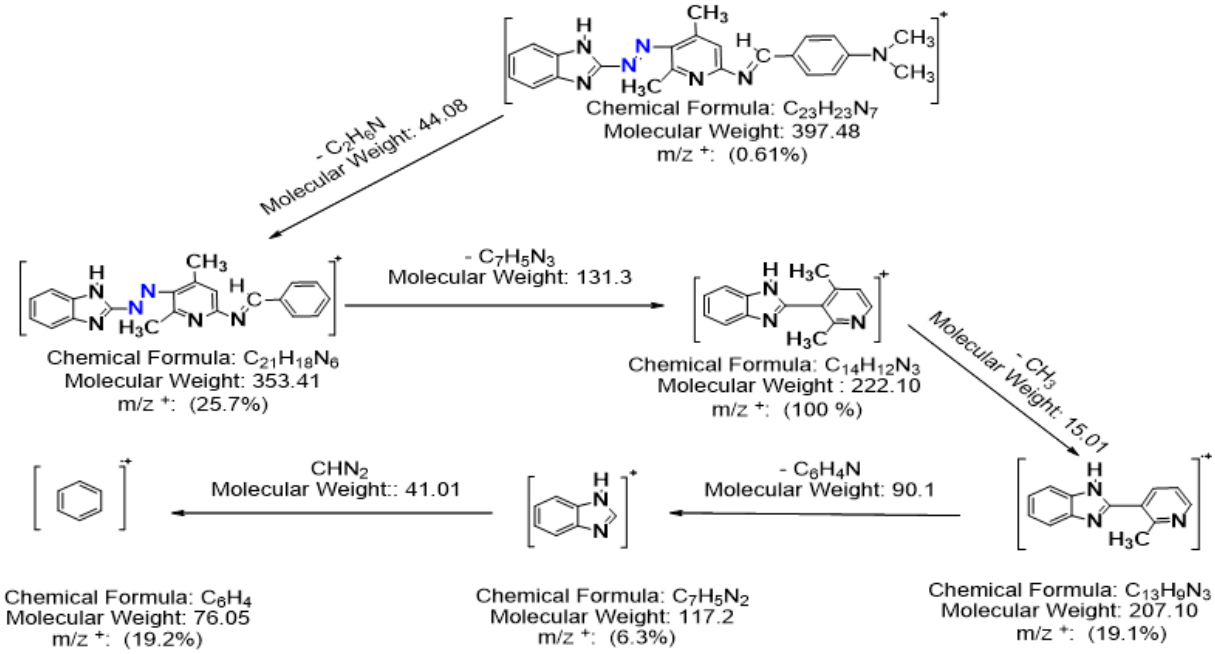

Scheme 2. Mass spectrum fragmentation of azo-schiff base (L_2)

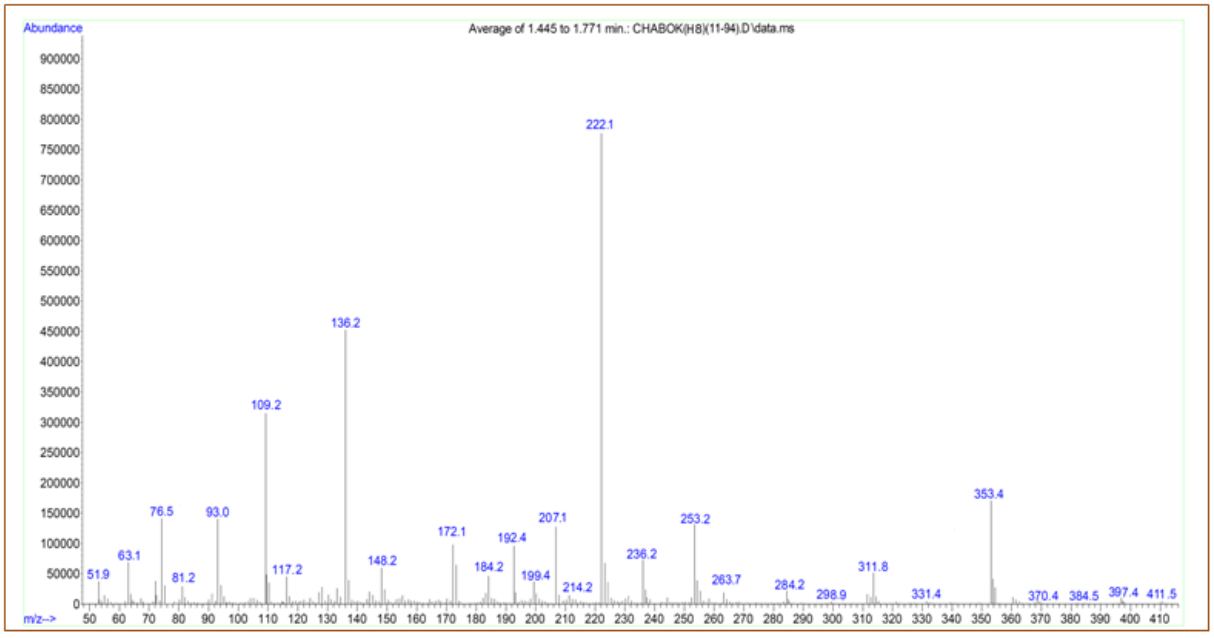

Figure 3. Mass spectrum of azo-schiff base (L_2)

Mass Spectra

The recorded mass spectrum of the ligand (L_2) (**Scheme 2**, **Figure 3**) and the molecular ion peaks have been used to confirm the proposed formula. The mass spectrum of ligand (L_2) showed several peaks attributed to the molecular ions at (m/z^+) 397.48 , 353.41 , 222.10 , 207.10 , 117.2 and 76.05 were due to various fragments ions $[C_{23}H_{23}N_7]^+$, $[C_{21}H_{18}N_6]^+$, $[C_{14}H_{12}N_3]^+$, $[C_{13}H_9N_3]^+$, $[C_7H_5N_2]^+$ and $[C_6H_4]^+$ respectively. This data is in good agreement with the corresponding molecular formulae [35].

The molecular ion peaks of Pd(II) - complex shows different m/z^+ values with different intensities. The mass spectrum contain molecular ion peaks at (m/z^+) 574.80, 528.5, 494.5 459,106.42,121.17, 91.9 and 51.0 were due to various fragments ions $[C_{23}H_{23}Cl_2N_7Pd]^+$, $[C_{21}H_{16}Cl_2N_6Pd]^+$, $[C_{21}H_{18}ClN_6Pd]^+$, $[C_{21}H_{17}N_6Pd]^+$, $[Pd^{+2}]$, $[C_7H_9N_2]^+$, $[C_6H_7N]^+$, and $[C_4H_4]$ respectively . This data is in good agreement with the corresponding molecular formulae [36].

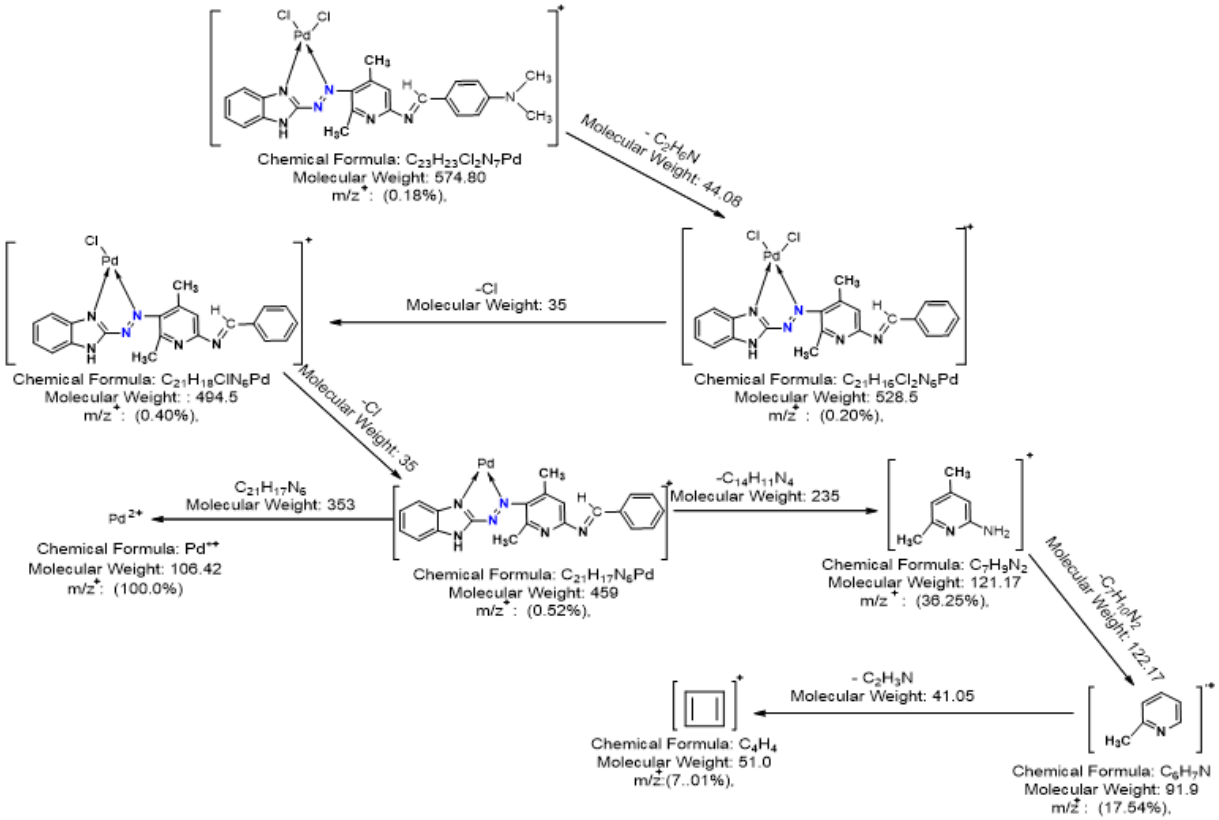

Scheme 3. Mass spectrum fragmentation of Pd-Complex:[Pd(L2)Cl2]

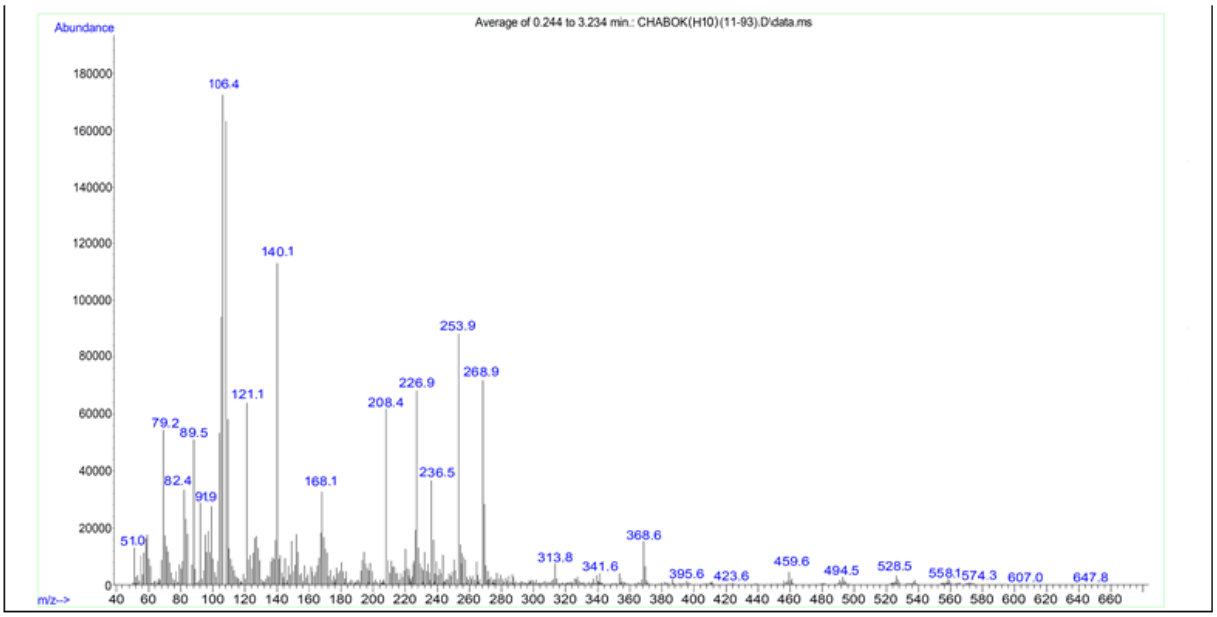

Figure 4. Mass spectrum of Pd-Complex:[Pd(L2)Cl2]

Infrared Spectra of Azo-schiff Base Ligand and their Metal Complexes

The IR spectrum of the ligand (L_2) is compared with the metal complexes in order to determine the coordination sites that may be involved in chelation. There are some guide bands, in the spectrum of the free ligand (L_2), which are of great help for achieving this goal. The position or the intensities of these bands are expected to be changed upon complex formation. The characteristic bands of the free ligand (L_2) and its metal complexes are discussed here. The IR spectrum of the ligand (L_2) exhibited a broad strong the band at 3442 cm^{-1}, which assigned to **υ**(N-H) stretching vibration of benzimidazol moiety, bands at 1635 cm^{-1} and 1558 cm^{-1} due to **υ**(C=N) in the new azo-schiff

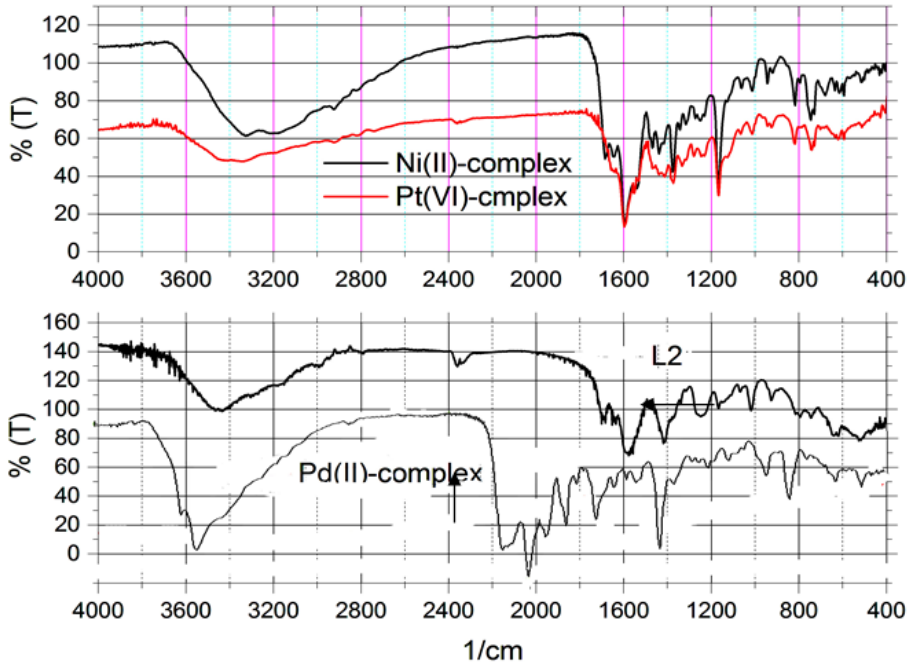

Figure 5. IR Spectrum of azo- schiff base dye ligand (L_2) and its metal complexes

Table 2. Selected infrared absorption bands (4000-400) cm^{-1} for azo- schiff base dye ligand (L_2) and its metal complexes (KBr disc)

Group	Ligand (L_2)	Ni(II)	Pd(II)	Pt(IV)
υH2O	-------	3325(sh.)	----------	---------
ν(NH)	3434(m.)	3217(sh.)	3444(sh.)	3409(sh.)
ν(C=N)	1635(w.)	1643(w.)	1677(s.)	1606(vs.)
ν(N=N)	1558(s.)	1438(s.)	1460(s.)	1459(m.)
ν(C=C)	1411(s.)	1438(w.)	1473(m.)	1373(s.)
ν(C-N)	1247(m.)	1249(w.)	1168(s.)	1164(vs.)
ν(M-N)	526(w.)	518(w.)	521(w.)	513(w.)

Vs = very strong , S = strong , m= medium , w = weak, sh = sholder,

base ligand and υ(C=N) of imidazole molecule vibrations, respectively. The appearance of a medium band in the IR spectrum of the ligand (L_2) at 1411 cm^{-1}, is ascribed to the stretching vibration of azo group (-N=N-). In comparison with the spectra of the metal complexes exhibited increase shift of about 15-25 cm^{-1} in the band of -(C=N) indicating the participation of azomethine nitrogen atom in coordination with the metal ions [34–36]. The most change in the schiff base spectral features when coordinated to metal ion is the change in shape, intensity and shifted frequencies of υ (N=N) stretching, indicates that azo group of the ligand (L_2) in coordinate to the metal ion through nitrogen atom, forming metal–nitrogen bond. The stretching vibration of the -(N=C) group of azo-schiff base ligand was not shifted more in the spectrum of metal complexes, thereby, indicating the non-participation of in complex formation. Furthermore, the appearance of new absorption bands at (513–523) cm^{-1} in the spectra of the metal complexes, indicated the formation M–N bonds, respectively [37]. The infrared spectra of new azo-schiff base ligand (L_2) and its metal complexes are shown in **Figure 5**.

Magnetic Susceptibility and Electronic Spectra Measurements

The UV–Visib. spectra were recorded in absolute ethanol solution (10^{-3} M) and absorption bands given in **Table 3** and **Figure 6**. The spectra of metal complexes are dominated by intense intra-ligand charge transfer bands. The spectrum of ligand (L_2) shows an intense absorption band at 417 nm (2390) cm^{-1} assigned to n→π* transition of azo and azomethine groups [38]. The geometries are supported by their electronic spectra.

The electronic spectrum of Ni(II) - complex exhibited three absorption bands at 978 nm(10225)cm^{-1}, 570 nm(17544)cm^{-1} and 432 nm(23148)cm^{-1}. These bands may be assigned to $^3A_2g \rightarrow {}^3T_2g_{(F)(\upsilon 1)}$, $^3A_2g \rightarrow {}^3T_1g_{(F)(\upsilon 2)}$ and $^3A_2g \rightarrow {}^3T_1g_{(p)(\upsilon 3)}$ transitions, respectively in an octahedral environment. The magnetic susceptibility for Ni(II) - complex shows a paramagnetic behavior and the μ_{eff} value equal 2.69 B.M. indicating the octahedral geometry because of the presence of two unpaired electrons (t_2g^6 eg^2) high-spin and sp^3d^2 hybrization [39].

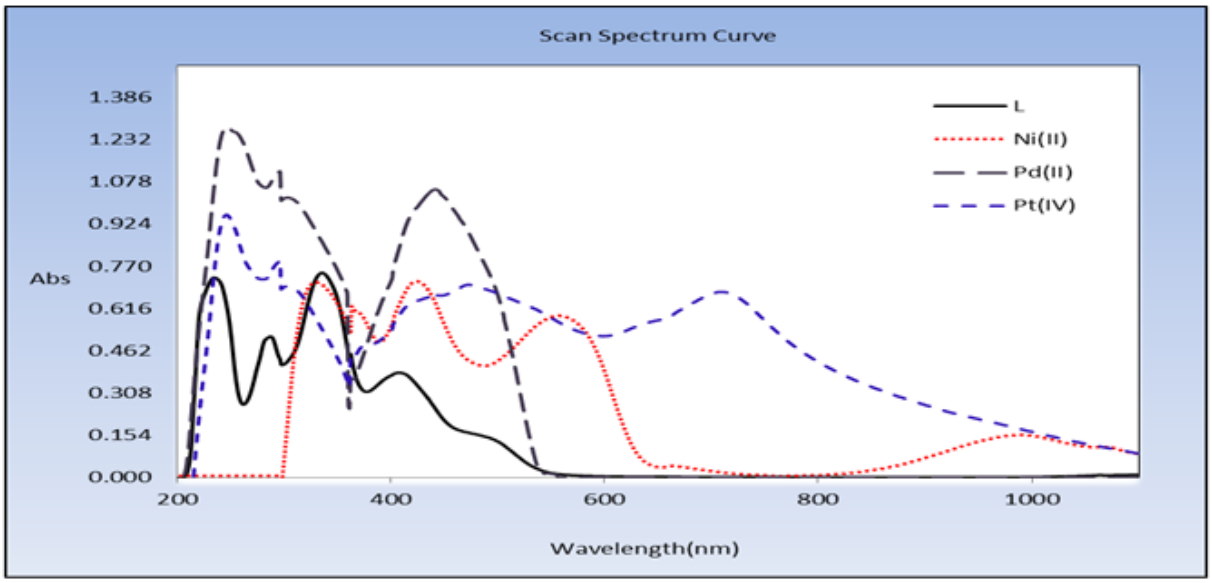

Figure 6. UV. Visb. spectra of ligand (L_2) and its metal complexes

Table 3. Electronic spectra (nm , cm^{-1}), magnetic moments, geometry and hybridization

Compounds	λ_{max} (nm)	Absorption bands(cm^{-1})	Transitions	μ_{eff} (B.M)	Geometry	Hybridization
Ligand=(L_2)	417	23981	n →π*	-------	----------	----------
	341	29325	π →π*			
	291	34364	π →π*			
$[Ni(L_2)_2Cl_2].H_2O$	978	10225	$^3A_2g \rightarrow {}^3T_2g_{(F)}$ ($_1\upsilon$)	2.69	Octahedral (Regular)	$sp^3\ d^2$ (High spin)
	570	17544	$^3A_2g \rightarrow {}^3T_1g_{(F)}$ ($_2\upsilon$)			
	432	23148	$^3A_2g \rightarrow {}^3T_1g_{(p)}$ ($_3\upsilon$)			
$[Pd(L_2)\ Cl_2]$	455	21978	$^1A_1g \rightarrow {}^1B_1g$	Dia	Square planer	dsp^2 (Low spin)
$[Pt(L_2)_2Cl_2]Cl_2$	719	13908	$^1A_1g \rightarrow {}^1T_1g_{(F)}$ ($_1\upsilon$)	Dia	Octahedral (Regular)	d^2sp^3 (Low spin)
	483	20704	$^1A_1g \rightarrow {}^1T_2g_{(F)}$ ($_2\upsilon$)			

B.M= Bohr magneton

The observed magnetic moment of the Pd(II)-complex is diamagnetic because of location of palladium is second round (d^8-low spin) and indicate a square planer geometry (hybridization dsp^2). Which confirms the square planar structure of this complex [34]. Electronic spectrum of the Pd (II)- complex displays band at 455 nm (21978 cm^{-1}) may be assigned to the transitions: $^1A_1g \rightarrow {}^1B_1g$ which is the sterochemistry for this complex a tetra coordinate. The Pd(II) complex may have either D_4h symmetry[40].

The electronic spectrum of the Pt(IV)-complex displays two bands at 483nm(20704) cm^{-1} and 719 nm(13908 cm^{-1}). These bands may be assigned to following transitions $^1A_1g \rightarrow {}^1T_1g_{(F)}$ $(_1\upsilon)$ and $^1A_1g \rightarrow {}^1T_2g_{(F)}$ $(_2\upsilon)$ respectively. This suggests an octahedral environment around the Pt(IV) ion.

Thermal Analysis

The thermal degradation of the azo-schiff base ligand and its metal complexes were investigated by thermogravimetric (TG) analysis, differential thermogravimetric (DTG) and differential scanning calorimetry (DSC) in the temperature range (22-705) ˚C. A representative TG, DTG, DSC diagram is given in **Figure 7**. The thermal stability data are listed in **Table 4**. The data from the thermogravimetric analysis clearly indicated that the decomposition of the complexes proceeds in two, three or four steps. Water molecules were lost in first step between 50 - 200 °C and metal oxides were formed above 600 °C for metal complexes. The decomposition was complete at ≥600 °C for all metal complexes.

From the TG curve of the Ni(II)-complex, it can be seen that decomposition starts at 90 ˚C and shows almost a continuous weight loss in the temperature range of 90-635 ˚C. Based on the percentage of mass losses and the DTG curve, four-step decomposition is proposed for this complex, which is similar to the decomposition pattern reported previously in the literature [43]. According to literature the azo bonds in the azo schiff base- metal complexes breakdown when the temperature is higher than 250 ˚C resulting in the endothermic peaks [44].The first

Table 4. Thermal analyses data for (TG,DTG,DSC) of ligand and metal complex

Compound	Dissociation stages	Temperature Range (˚C)	Mass loss Found (calcd.) (%)	DTG peak (˚C)	DSC peak (˚C)	Decomposition assignment	Residue
Ligand=L_2	Stage I	200-600	98(100)	312	310	The gradual loss of ($C_8H_{11}N$) N,N dimethylaniline and residual ligand molecule	---
Ni(II)-complex	Stage I	90-150	2.3 (1.91)	128	120	The loss of H_2O	**NiO**
	Stage II	150-320	10.0 (9.33)	260	245	The loss of 2 Cl	
	Stage III	320-400	24.0 (22.10)	372	361	The loss of 8 CH_3	
	Stage VI	400-580	91.0 (93.59)	482	479	The loss of residual ligand	
Pd(II)-complex	Stage I	210-318	13.0 (12.19)	230	223	The loss of 2Cl	**PdO**
	Stage II	318-400	34.0 (32.19)	346	341	The loss of ($C_7H_6N_2$) benzimidazol	
	Stage III	400-580	79.0 (75.98)	531	529	The loss of residual ligand	
Pt(VI)-complex	Stage I	100-150	7.0 (6.27)	131	139	The loss of the 2Cl molecule outer-sphere coordination	**Pt O_2**
	Stage II	150-300	14.0 (12.54)	251	253	The loss of the 2Cl molecule inner -sphere coordination	
	Stage III	300-455	33.0 (33.75)	382	380	The loss of ($C_8H_{11}N$) N,N-dimethylaniline	
	Stage VI	455-611	80.0 (81.19)	531	529	The loss of residual ligand	

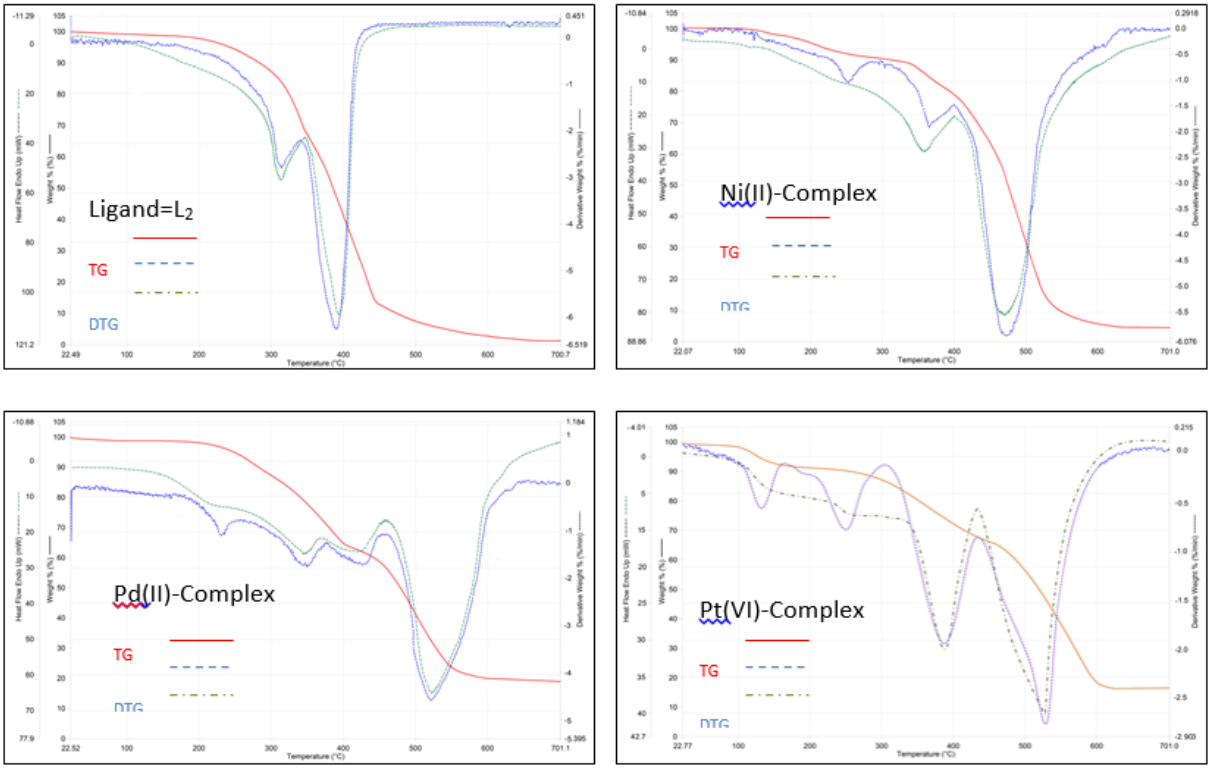

Figure 7. TG-DTG-DSC curves of ligand (L_2) and their complexes

decomposition step with an estimated mass loss of 2.3% within the temperature range (90-150)˚C may be attributed to the loss of H_2O molecule (calcd. 1.91%). The DTG peak corresponding to this stage is at 128˚C and the recorded DSC curve reveals a sharp endothermic peak at 120˚C. The second step at range (150-320) °C of decomposition an estimated mass loss of 10.0%, (calcd. 9.33%) corresponds to the elimination of 2Cl atoms. recorded DTG curve a sharp peak at 260˚C and DSC curve at 245˚C. The third decomposition stage within the temperature range of (320-400) °C with mass loss of 24% (calcd. 22.1%) due to the elimination of 8CH_3. The DTG exhibit peak corresponding to this stage is at 372˚C DSC curve shows endothermic peaks at 361˚C. The final decomposition stage in the temperature range 400-580 °C with mass loss of 91% (calcd. 93.59%) due to the elimination of the residual ligand molecules, NiO as a final product. The DTG and DSC curves exhibit sharp peaks at 482 ˚C and 479 ˚C respectively.

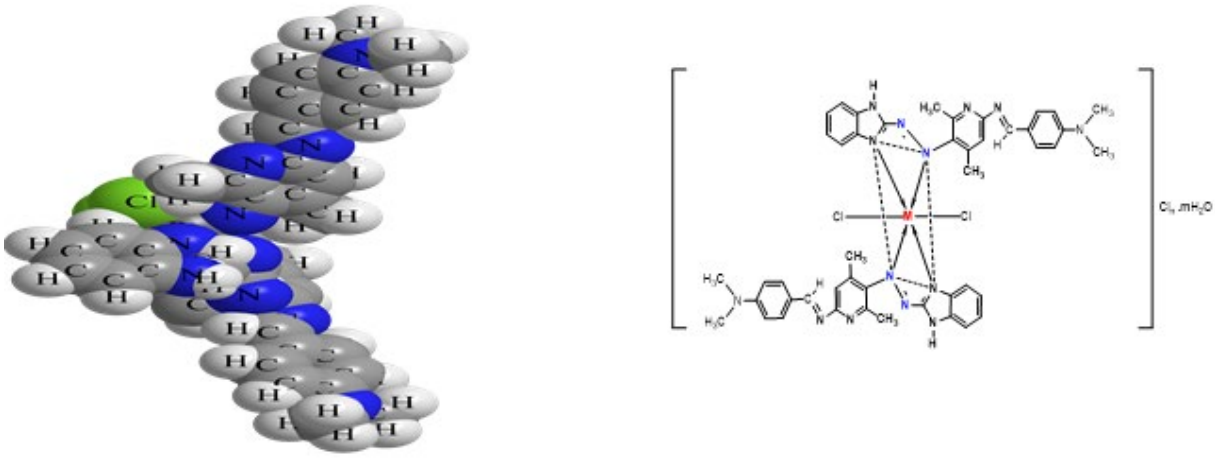

Figure 8. The proposed chemical structure formula of the metal **complexes when:-**
M= Ni (II) ; n=0, m=1
M= Pt (IV); n=2, m=0

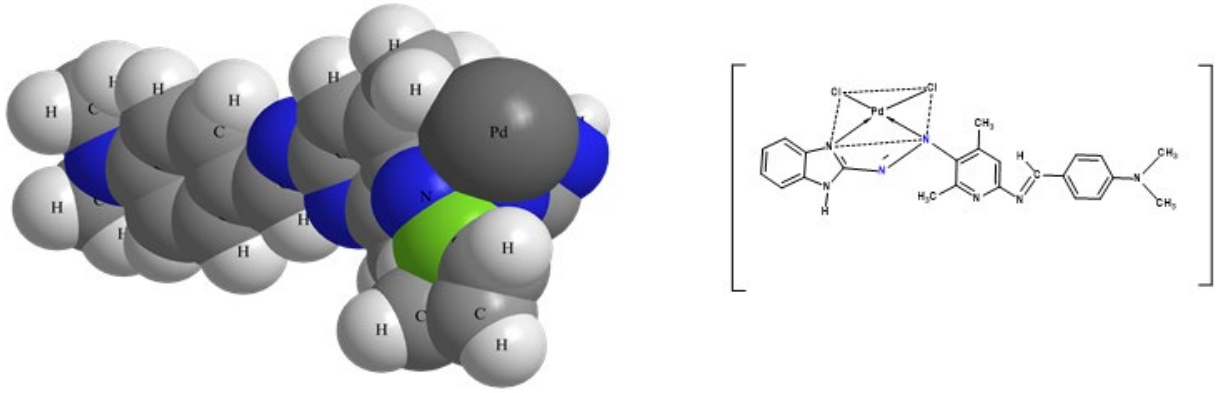

Figure 9. The proposed chemical structure formula of the Pd(II)-complex

The Pd(II)-complex is thermally decomposed in four successive decomposition steps within the temperature range (22.5-705.0) ˚C. The first decomposition step of estimated mass loss 13 % within the temperature range (210-318)˚C may be attributed to the loss of the 2Cl atoms (calcd. 12.19%). DTG peaks corresponding to this stage are observed at 230 ˚C. Simultaneously, the recorded DSC curve reveals a broad endothermic peak at 223˚C. The second step at the temperature range (318-400)˚C with the mass loss 34% corresponds to the loss of the $C_7H_6N_2$ benzimidazol molecule (calcd. 32.19%). This decomposition process shows a broad peak at 346 and 341 ˚C in the DTG and DSC curve respectively. The third step found within the temperature range 400-580˚C with an estimated mass loss 79% which may be attributed to the loss of residual ligand molecule and PdO as a final product. (calcd. 75.98%). The broad DTG peak corresponding to this step is observed at 531˚C. The recorded DSC curve shows peak at 529 ˚C.

The Pt(VI)-complex is thermally decomposed in four decomposition steps. The first decomposition step of estimated mass loss 7% within the temperature range (100-150) ˚C with an estimated mass loss of the Cl molecule outer-sphere coordination (calcd. 6.27%). The DTG sharp peak corresponding to this stage is observed at 131˚C. The recorded DSC curve peak at 139 ˚C. The second step occurs within the temperature range (150-300)˚C with a DTG peak at 251 ˚C, may be attributed to the loss 14% (calcd. 12.54%), which may be due to loss of the 2Cl molecule inner-sphere coordination, The complex also shows third step displays a mass loss of 33% (calcd. 33.75%), within the temperature range 300-455˚C with a DTG peak at 382˚C, which may be attributed to the loss of the 2($C_8H_{11}N$) N,N-dimethylaniline molecule. The recorded DSC curve reveals an endothermic peak at 380˚C. The final decomposition step in the temperature range (455-611) ˚C exhibits a loss in mass of 80% (calcd. 81.19%), which may be attributed to the complete decomposition of a part of ligand molecule. This step shows obvious peaks in the DTG and DSC curves 531 ˚C and 529 ˚C respectively.

According to these results and discussed the data through different techniques suggest the structural formula of prepared metal complexes in this work may be proposed in **Figures 8** and **9**.

Table 5. Inter planar distances , 2θ value, FWHM and Crystallite Size of each peak, relative intensity for ligand and complexes

Compound	*2* θ Obs. (degree)	d calc. spacing (A°)	FWHM [°*2* θ]	Crystallite Size D(nm)
Ligand=L_2	31.889	2.8041	0.2131	0.6588
	45.513	1.9893	0.1643	0.8910
	54.081	1.6944	0.1437	1.0547
	63.272	1.9686	0.2754	0.5757
Ni(II)-complex	31.971	2.7970	0.1753	0.8010
	45.574	1.9882	0.1874	0.7813
	53.497	1.7115	0.1021	1.3883
Pd(II)-complex	31.889	2.8041	0.1364	1.0766
	45.488	1.9924	0.1175	1.2458
	53.782	1.7031	0.1312	1.1537
	73.659	1.2850	0.2123	0.7944
Pt(VI)-complex	31.739	2.8170	0.1764	0.7956
	45.563	1.9893	0.1548	0.9458
	54.007	1.6965	0.1032	1.4682

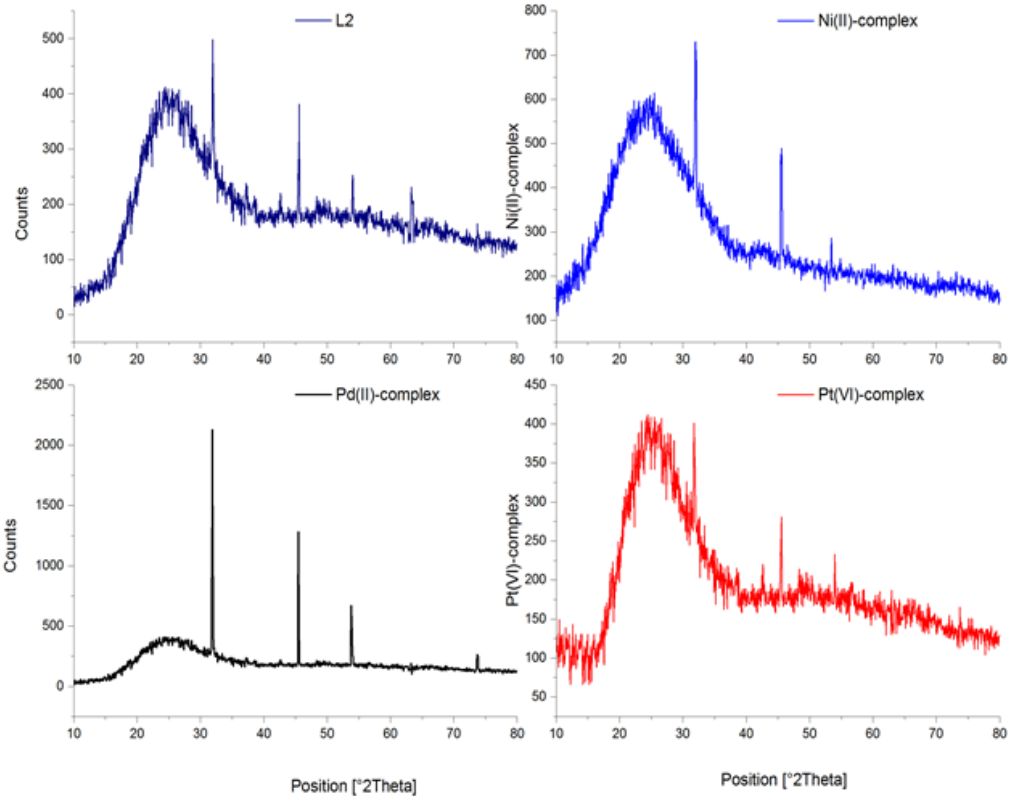

Figure 10. X-ray diffraction patterns for ligand (L_2) and its metal complexes

X-ray Diffraction Analysis

The X-ray diffraction, XRD, patterns of the ligand (L_2) and its metal complexes $[Ni(L_2)_2Cl_2].H_2O$, $[Pd(L_2)\ Cl_2]$ and $[Pt(L_2)_2Cl_2]\ Cl_2$ are shown in **Figure 10**. The XRD patterns of the ligand (L_2) and Ni(II), Pd(II) and Pt(IV)-complexes have sharp diffraction peaks at around 2θ=30–80, this indicates that ligand (L_2) and complexes are a mixture of crystalline and amorphous phases. While the XRD pattern of Pt(IV)-complex is very less mixture of crystalline and amorphous phase. Calculate d-spacing or 'd' values of reflections were obtained using Bragg's equation $n\lambda = 2dsin\ \theta$ [45], The average size of the particles and their size distribution were evaluated by the Scherer equation, $D = k\lambda/\beta Cos\theta$, The values in **Table 6**.

SEM Studies

Scanning electron microscopy (SEM) of the azo-schiff base ligand (L_2) and Pd(II)- complex studies the surface morphology and shape of the particles and aggregation, in addition to the distribution of these particles. The SEM

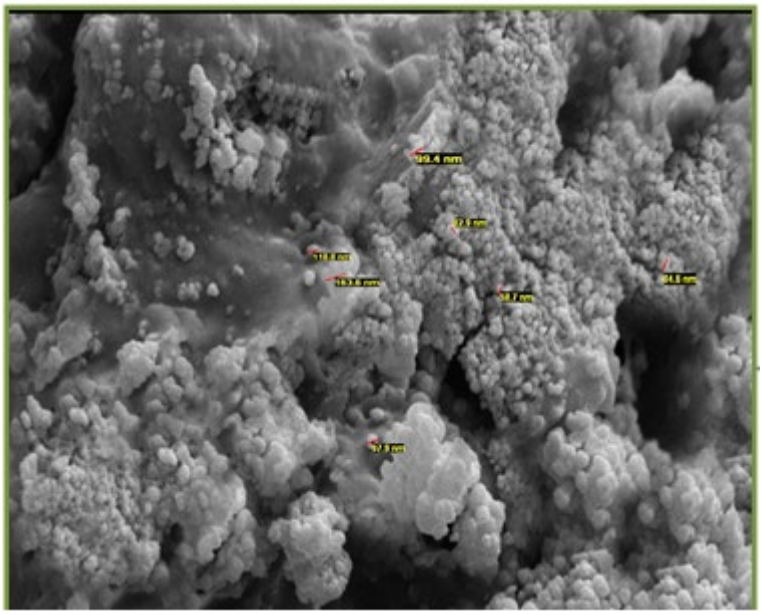

Figure 11. Scanning electron micrographs of [Pd(L_2) Cl_2]

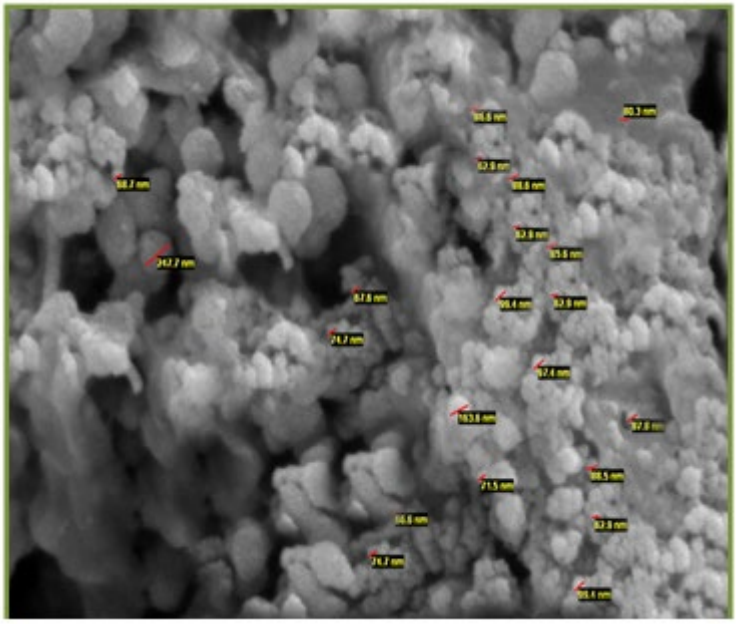

Figure 12. Scanning electron micrographs of azo-schiff base ligand

image of ligand (L_2) and [Pd(L_2) Cl_2] have been illustrated in **Figures 11** and **12**. SEM image shows the ligand (L_2) have form of peripheral spherical shape with average size 91.22 nm with a ratio of less than aggregation. The SEM image of Pd(II)-complex appeared in the form of heterogeneous the surface with average particle size 86.64 nm. According to the images of SEM different characteristic shapes of Pd(II)- complex was identified and these SEM images were different from that of azo-schiff base ligand (L_2). We can be seen that Pd(II)- complex gave a aggregation less than azo-schiff base ligand.

PHARMACLOG RESULTS

Antibacterial Activity

In this study we investigated antibacterial activity of the azo-schiff base and its series of metal complexes Ni(II),Pd(II) and Pt(IV) were screened for antibacterial activity against microorganisms representing Gram-positive bacteria [*Staphylococcus aureus*] and Gram - negative bacteria [*Escherichia coli*] ,by agar diffusion method. DMSO is

Table 6. Antibacterial activity of ligand (L_2) and its complexes

Comp. No.	Anti - bacterial Activity		Anti - fungal Activity
	E. coli	Staphylococcus	Alternaria
Ligand=(L_2)	-	-	-
[$Ni(L_2)_2Cl_2$].H_2O	-	-	+
[$Pd(L_2)$ Cl_2]	-	-	++
[$Pt(L_2)_2Cl_2$]Cl_2	-	-	-

(+++)Highactive-Inhibition zone>12mm , (++) Moderate active-Inhibition zone=9-12mm.
(+)Slightly active-Inhibition zone=6-9mm , (-)Inactive <6mm

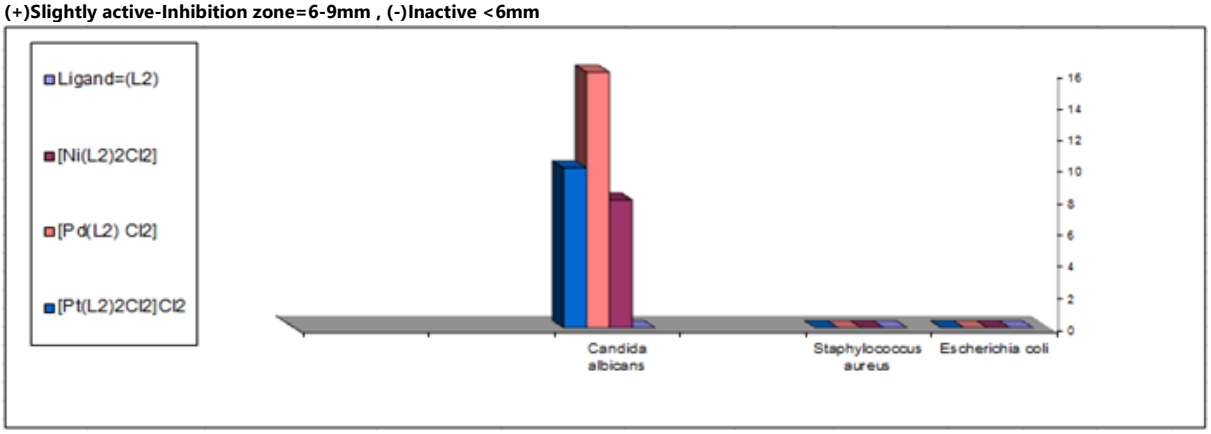

Figure 13. Minimum Inhibitory concentration (MIC) in molar concentration ($1x10^{-4}$ M) of the ligand (L2) and its metal complexes

used as solvent. All the compounds were inoculated using a loop onto plates containing Nutrient Agar (NA) media and incubated at 32°C for 24 hours. To carry out agar diffusion assay the bacterial suspensions were prepared in sterile distilled water [47-49]. The ligand and its metal complexes not have bacterial activity against both bacterial. The results of the antimicrobial activity of the ligand and its metal complexes against all tested bacterial are shown in **Figure 13** and **Table 6**.

Antifungal

The antifungal activity of ligand and its metal complexes have been studied by agar diffusion method against the fungi Alternaria. Flucanozole is used as standard antibiotic and DMSO is used as solvent [50-52]. The antifungal activity of the azo-schiff base and metal complexes against the fungi Alternaria are shown in **Table 6** and **Figure 13**.

Cell Viability and Cytotoxicity Assay

In this analytical method that was primarily developed by Mosmsnn [53-55], the density of cells can be determined based on cell color in small volumes after converting spheroids to single cells, two different densities of single cells including 8000 and 10,000 cells in different plates were selected for MTT assay. After a period of 24 hrs. dissolved MTT in PBS with final density of 0.5 mg/ml was added and after incubation for 4 hrs. MTT solution was extracted and DMSO was then added and was shaken for 20 min. Finally, absorption of the samples was read by regulating 570 nm filter as the main wavelength and also 630 nm filter as the referenced wavelength. The absorption rate of the wells without cells was diminished from absorption of the wells with cells to obtain pure cellular absorption. According to the following equation, there is a direct association between pure absorption and rate of viable cells:

(Mean absorption of sample / mean absorption of referenced)×100=percentage of viable cells. The in vitro cytotoxicity of the Pd(II)-complex, on human cell lines PC3 was used to determine the antiproliferative effect of synthesized compound. The selectivity index (SI), which indicates the cytotoxic selectivity of the compound against cancer cells and its safety towards the normal cells, was determined from the ratio of the *IC_{50} values were calculated for each cell line **Table 7** and **Figures 14** and **15**, Pd(II)-complex showed selective cytotoxicity against cancer cell line with IC_{50} = 425 µg/ml, while it was very safe on normal cells line with IC_{50} = 14554885 µM/ml, respectively for human cells.

IC_{50} =median inhibitory concentration is the concentration which causes 50% inhibitory effect on cellular proliferation

Table 7. IC_{50} (µg/ml) values and percentage (%) of the synthesized compound and standard drugs

Test samples	IC_{50} (µg/ml)				
	Carcinoma Cell Lines			Normal Cell Line	
	425			14554885	
	Mean Percentage (%) for each cell line				
	Conc. (µg/ml)	Carcinoma Cell Lines		Normal Cell Line	
		Cell Viability	Cell Inhibtion	Cell Viability	Cell Inhibtion
Pd(II)-complex	400	51.739	48.261	89.941	10.059
	200	74.69233	25.30767	94.32867	5.671333
	100	91.225	8.775	91.70667	8.293333
	50	94.168	5.832	95.024	4.976
	25	95.45233	4.547667	93.954	6.046
	12.5	96.522	3.478	92.40233	7.597667
	6.25	98.18067	1.819333	99.037	0.963

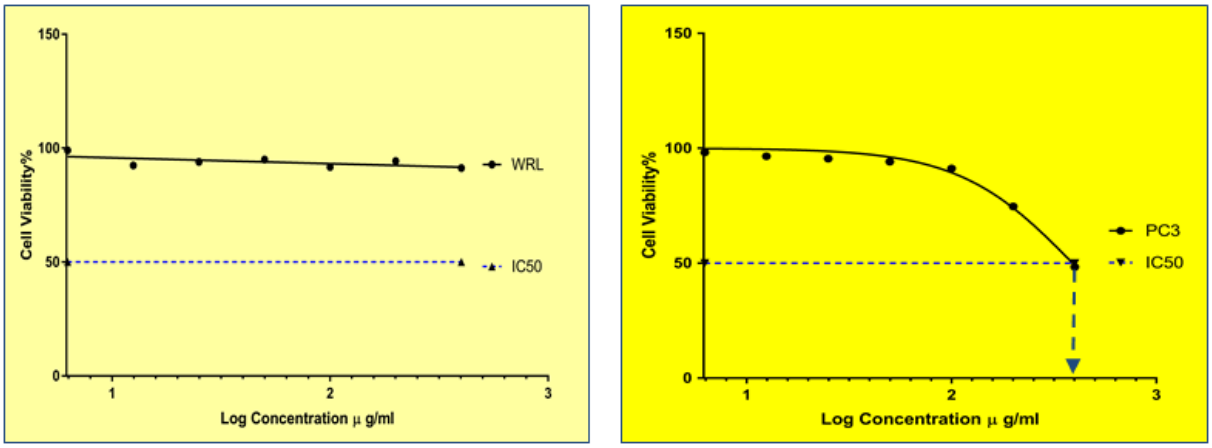

Figure 14. IC_{50} (µg/ml) values of the carcinoma cell lines normal cell Line

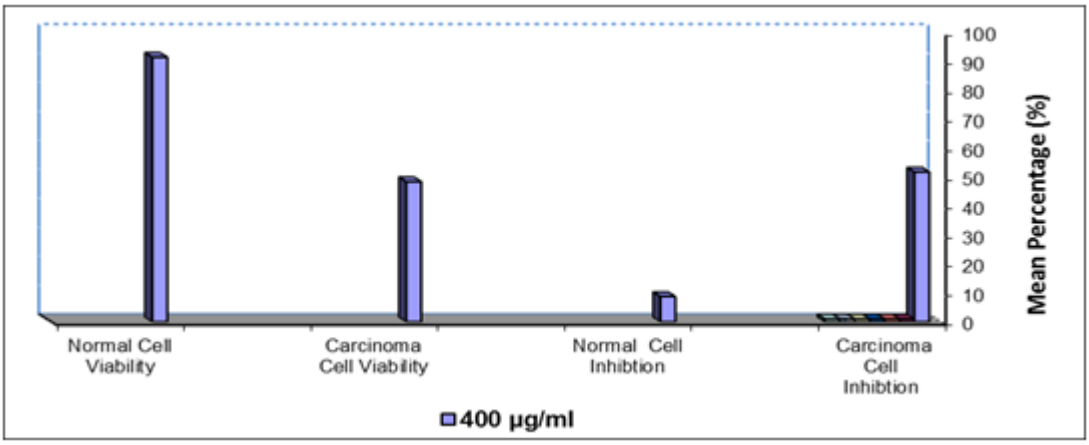

Figure 15. Comparison of viability and Inhibtion for each cell line (10000 cellular density)

Treating Tumors or Tumor Metastases

Killing cancer cells because of DNA binding cannot account for a selective mechanism of cell recognition and of discriminating toxicity. Provided that tumor cells differ from their healthy counterparts for the activated genes rather than for DNA content (which is almost identical in terms of nucleotide content, e.g. the number of guanines and their sequence, in any cell of the body including the tumor mass), the question remains open why, besides the high sensitivity of testicular tumors that can be cured, other tumors towards which platinum drugs are applied in a number of combination chemotherapeutic regimens show [56]. The mechanism of tumor cell killing by pladinum drugs have been illustrated in **Figure 16**.

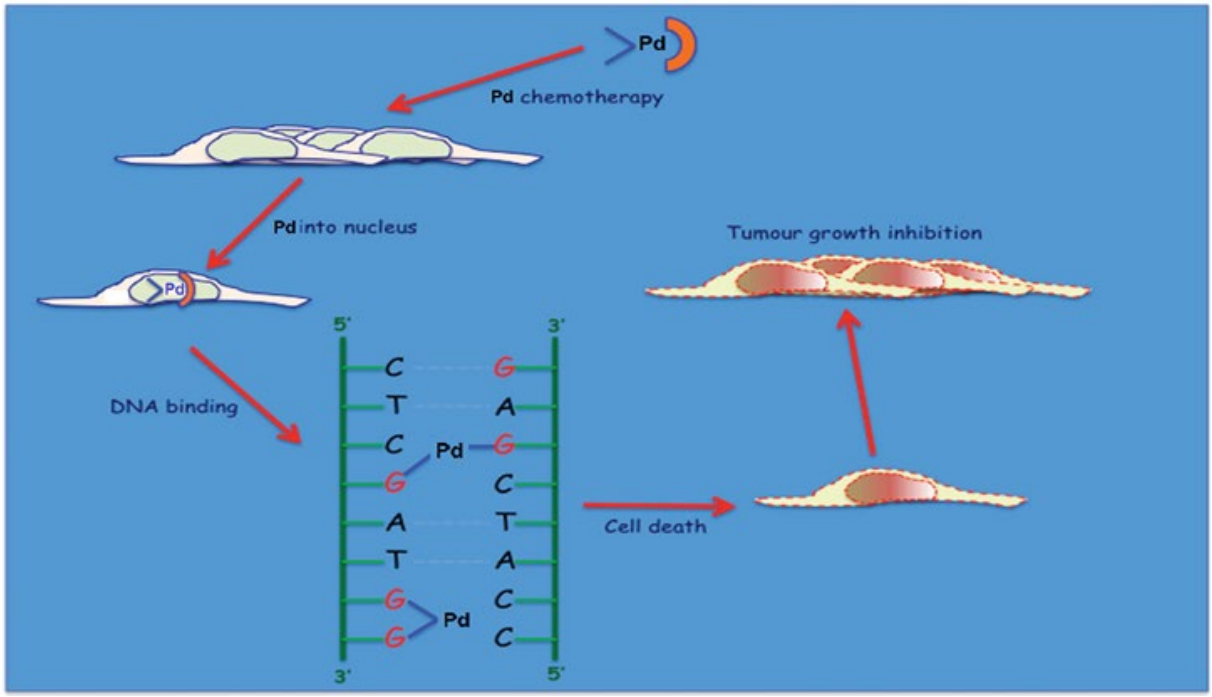

Figure 16. Schematic representation of the mechanism of tumour cell killing by pladinum drugs. The pladinum ion enters tumour cells, reaches their nucleus and binds to two adjacent guanines (making bridges on the same strand or between both strands). If repair mechanisms have no success on the adduct Pd-DNA then cell death occurs

CONCLUSION

In summary, new azo-schiff base ligand and its metal complexes were synthesized and characterized. Elemental analyses confirm the chemical composition of the synthesized compounds while FT-IR, mass, ^{1}H-NMR spectroscopy confirms the functional groups, particularly –N=N– and –HC=N imine groups, of the ligand. The metal- to-ligand ratio [M:L] of the Ni(II) and Pt(IV) complexes was [1:2],but for metal ion Pd(II) was found to be [1:1] and, thus, azo-schiff base ligand appears bidentate coordinated with the metals complexes. Crystal structures of the azo-schiff base ligand and its metal complexes were successfully determined by single-crystal X-ray diffraction. In the biological and antifungal activity studies, some synthesized compounds exhibit antimicrobial properties. The cytotoxicity of Pd(II)-complex on human (PC3) cancer and normal cells were studied using MTT assay. Pd(II)-complex showed higher selective cytotoxicity against cancer cell line, while it was very safe on normal cells line. The results indicate undoubtedly the possibility of using them as prostate cancer drugs in the field of medicine.

REFERENCES

1. Al-Hamdani AAS, Al Zoubi W. New metal complexes of N3 tridentate ligand: Synthesis, spectral studies and biological activity. Molecular and Biomolecular Spectroscopy. 2015;137:75–89. https://doi.org/10.1016/j.saa.2014.07.057
2. Uruş S, Adigüzel H, İncesu M. Synthesis of novel N4O4 type bis(diazoimine)-metal complexes supported on mesoporous silica: Microwave assisted catalytic oxidation of cyclohexane, cyclooctane, cyclohexene and styrene. Chemical Engineering Journal. 2016;296:90–101. https://doi.org/10.1016/j.cej.2016.03.101
3. Diab MA, El-Sonbati AZ, El-Bindarya AA, Morgan ShM, Abd El-Kader MK. Geometrical structures, molecular docking, spectroscopic characterization of mixed ligand and Schiff base metal complexes. Journal of Molecular Liquids. 2016;218:571–585. https://doi.org/10.1016/j.molliq.2016.01.102
4. Alaghaz A-NMA, Zayedb ME, Alharbib SA, Ammarc RAA, Elhenawya A. Synthesis, characterization, biological activity, molecular modeling and docking studies of complexes 4-(4-hydroxy)-3-(2-pyrazine-2-carbonyl)hydrazonomethylphenyl-diazen-yl-benzenesulfonamide with manganese(II), cobalt(II), nickel(II), zinc(II) and cadmium(II). Journal of Molecular Structure. 2014;1084:352-367. https://doi.org/10.1016/j.molstruc.2014.12.041

5. Ghasemian M, Kakanejadifard A, Karami T. Synthesis, structural characterization, antimicrobial activities and theoretical investigations of some 4-(4-aminophenylsulfonyl) phenylimino) methyl)-4-(aryldiazenyl) phenol. Spectrochimica Acta Part A: Molecular and Biomolecular Spectroscopy. 2016;16:190-198. https://doi.org/10.1016/j.saa.2016.06.007
6. Al-Khodir FAI, Refat MS. Synthesis, spectroscopic, thermal and anticancer studies of metal-antibiotic chelations: Ca(II), Fe(III), Pd(II) and Au(III) chloramphenicol complexes. Journal of Molecular Structure. 2016;1119: 157-166. https://doi.org/10.1016/j.molstruc.2016.04.069
7. Lazarević T, Rilakb A, Bugarčić ŽD. European Journal of Medicinal Chemistry. 2016;17:1-73.
8. Rubino S, Busà R, Attanzio A, Alduina R, Stefano VD, Girasolo MA, Orecchio S, Tesoriere L. Bioorganic & Medicinal Chemistry. 2016;16:1-25.
9. Kataki S, Hazarika S, Baruah DC. Investigation on by-products of bioenergy systems (anaerobic digestion and gasification) as potential crop nutrient using FTIR, XRD, SEM analysis and phyto-toxicity test. Journal of Environmental Management. 2017;196:201-216. https://doi.org/10.1016/j.jenvman.2017.02.058
10. Moodley S, Koorbanally NA, Moodley T, Ramjugernath D, Pillay M. The 3-(4,5-dimethylthiazol-2-yl)-2,5-diphenyl tetrazolium bromide (MTT) assay is a rapid, cheap, screening test for the in vitro anti-tuberculous activity of chalcones. Journal of Microbiological Methods. 2014;104:72–78. https://doi.org/10.1016/j.mimet.2014.06.014
11. Al-Adilee KJ, Abass AK, Taher AM. Synthesis of some transition metal complexes with new heterocyclic thiazolyl azo dye and their uses as sensitizers in photo reactions. Journal of Molecular Structure. 2016;1108:378-397. https://doi.org/10.1016/j.molstruc.2015.11.038
12. Li S, Song R-J, Wangb D-H, Tian X, Shao X-S, Zhong L. Azopyridine-imidacloprid derivatives as photoresponsive neonicotinoids. Chinese Chemical Letters. 2016;27(5):635–639. https://doi.org/10.1016/j.cclet.2016.03.033
13. Piyasaengthong A, Boonyalai N, Suramitr S, Songsasen A. Synthesis, characterization, and pepsin inhibition study of Au(III)–3-(2′-thiazolylazo)-2,6-diaminopyridine complex. Inorganic Chemistry Communications. 2015;59:88–90. https://doi.org/10.1016/j.inoche.2015.06.025
14. Amruthraj NJ, Preetam Raj JP, Saravanan S, Antoine Lebel L. International Journal of Pharmacy and Pharmaceutical Sciences. 2014;6:254-258.
15. McCauley J, Zivanovic A, Skropeta D. Bioassays for Anticancer Activities. Methods in Molecular Biology. 2013;1055:191-205. https://doi.org/10.1007/978-1-62703-577-4_14
16. Shi Y, Chu W, Wang Y, Wang S, Du J, Zhang J, Li S, Zhou G, Qin X, Zhang C. Synthesis, characterization and cytotoxicity of the Au(III) complexes with cyclic amine-based dithiocarbamate ligands. Inorganic Chemistry Communications. 2013;30:178–181. https://doi.org/10.1016/j.inoche.2013.02.010
17. Sánchez Delgado GY, Paschoal D, Dos Santos HF. Computational & Theoretical Chemistry. 2017;271:1-28.
18. Niedzielska D, Pawlak T, Bozejewicz M, Wojtczak A, Pazderski L, Szlyk E. Structural and spectroscopic studies of Au(III) and Pd(II) chloride complexes and organometallics with 2-benzylpyridine. Journal of Molecular Structure. 2013;1032:195–202. https://doi.org/10.1016/j.molstruc.2012.08.005
19. Ammar RA, Alaghaz A-NMA, Zayed ME, Al-Bedair LA. Journal of Molecular Structure. 2017;2860:1-40.
20. Pradeepa SM, Bhojya Naik HS, Vinay Kumar B. Molecular and Biomolecular Spectroscopy. 2015;1425:1-40.
21. Joseph J, Boomadevi Janaki G. Copper complexes bearing 2-aminobenzothiazole derivatives as potential antioxidant: Synthesis, characterization. Journal of Photochemistry & Photobiology, B: Biology. 2016;162:86–92. https://doi.org/10.1016/j.jphotobiol.2016.06.030
22. Al-Adilee KJ. Research Journal of Pharmaceutical, Biological and Chemical Sciences. 2015;6:1297-1308.
23. Al-Adilee KJ, Hessoon HM. J. Chem. Pharm. Res. 2015;7(8):89-103.
24. Al-Adilee KJ, Kyhoiesh HAK. Preparation and identification of some metal complexes with new heterocyclic azo dye ligand 2-[2−- (1- Hydroxy -4- Chloro phenyl) azo]- imidazole and their spectral and thermal studies. Journal of Molecular Structure. 2017;1137:160-178. https://doi.org/10.1016/j.molstruc.2017.01.054
25. Kose M, Hepokur C, Karakas D, McKee V, Kurtoglu M. Polyhedron. 2016;16:1-30.
26. Zianab T, Khammas ZAA, Al-Adilee KJ. Int. J. Chem. Sci. 2014;12(4):1189-1207.
27. Alaghaz A-NMA, Zayed ME, Alharbi SA. Journal of Molecular Structure. 2014;14:1-19.
28. Hashemi M, Solati Z, Ghodsi A, Ahmadian S. Synthetic Metals. 2015:1–6.
29. Al-Adilee KJ, Dakhil HK, Karam FF. J. AL-Qadisiya Pure Sci. 2011;16:50-62.
30. Kantar C, Mavi V, Baltaş N, İslamoğlu F, Şaşmaz S. Journal of Molecular Structure. 2016;16:1-40.
31. Al-Adilee KJ, Al-Shamsi HAH, Dawood MN. Res. J. Pharm. Bio. Chem. Sci. 2016;7(4):2882-2905.
32. Shafaatian B, Mousavi SS, Afshari S. Synthesis, characterization, spectroscopic and theoretical studies of new zinc(II), copper(II) and nickel(II) complexes based on imine ligand containing 2-aminothiophenol moiety. Journal of Molecular Structure. 2016;1123:191–198. https://doi.org/10.1016/j.molstruc.2016.06.033

33. Al-Adilee KJ, Hatem BA. J. Advance in Chem. 2015;11(3):3412-3425.
34. Pal MK, Kushwah N, Wadawale AP. Synthesis, characterization, photoluminescence and computational studies of mono- and diorgano-gallium complexes containing azo linked salicylaldimine Schiff bases. J. of Organometallic Chemistry. 2015;776:98-106. https://doi.org/10.1016/j.jorganchem.2014.10.024
35. Mathammal R, Sangeetha K, Sangeetha M, Mekala R, Gadheeja S. Synthesis, crystal structure analysis, spectral IR, NMR UV–Vis investigations, NBO and NLO of 2-benzoyl-N-(4-chlorophenyl)-3-oxo-3-phenylpropanamide with use of X-ray diffractions studies along with DFT calculations. Journal of Molecular Structure. 2016;1118:316-324. https://doi.org/10.1016/j.molstruc.2016.04.042
36. Demir S, Guder A, Yazıcılar TK, Çaglar S, Buyukgungor O. Syntheses, crystallographic, mass-spectroscopic determination and antioxidant studies of Co(II), Ni(II) and Cu(II) complexes of a new imidazol based Schiff base. Spectrochim. Acta Part A. 2015;150:821–828. https://doi.org/10.1016/j.saa.2015.06.023
37. Biswas S, Acharyya S, Sarkar D, Gharami S, Mondal TK. Spectrochimica Acta. 2016;16:1-25.
38. Mostafa A, El-Ghossein N, Cieslinski GB, Bazzi HS. UV–Vis, IR spectra and thermal studies of charge transfer complexes formed in the reaction of 4-benzylpiperidine with σ- and π-electron acceptors. Journal of Molecular Structure. 2013;1055:199-208. https://doi.org/10.1016/j.molstruc.2013.09.007
39. Özdemir Ö. Journal of Molecular Structure. 2016;16:1-46.
40. El-Bindary AA, El-Sonbati AZ, Diaba MA. Polymeric complexes — LXII. Coordination chemistry of supramolecular Schiff base polymer complexes — A review. Journal of Molecular Liquids. 2016;216:318–329. https://doi.org/10.1016/j.molliq.2015.12.113
41. Srivastva AN, Singh NP, Shriwastaw CK. Arabian Journal of Chemistry. 2014;14:1-42.
42. Valamary G, Subbalaksmi R. Indian J. Appl. Res. 2013;3:43-49.
43. El-Sonbati AZ, Diab MA, El-Bindarya AA, Mohamed GG, Morgan SM, Abou-Dobara MI, Nozh SG. Geometrical structures, thermal stability and antimicrobial activity of Schiff base supramolecular and its metal complexes. Journal of Molecular Liquids. 2016;215:423–442. https://doi.org/10.1016/j.molliq.2015.12.006
44. Karaagaç D, Kürkçüoglu GS. Syntheses, spectroscopic and thermal analyses of cyanide bridged heteronuclear polymeric complexes: [M(L)2Ni(CN)4]n (LN-methylethylenediamine or N-ethylethylenediamine; MNi(II), Cu(II), Zn(II) or Cd(II)). Journal of Molecular Structure. 2016;1105:263-272. https://doi.org/10.1016/j.molstruc.2015.10.023
45. Masoudiasl A, Montazerozohori M, Naghiha R, Assoud A, McArdle P, Shalamzari MS. Synthesis, X-ray crystal structures and thermal analyses of some new antimicrobial zinc complexes: New configurations and nano-size structures. Mate. Sci. Eng. 2016;61:809–823. https://doi.org/10.1016/j.msec.2016.01.017
46. Shakir M, Hanif S, Sherwani MA, Mohammad O, Al-Resayes SI. Pharmacologically significant complexes of Mn(II), Co(II), Ni(II), Cu(II) and Zn(II) of novel Schiff base ligand, (E)-N-(furan-2-yl methylene) quinolin-8-amine: Synthesis, spectral, XRD, SEM, antimicrobial, antioxidant and in vitro cytotoxic studies. Journal of Molecular Structure. 2015;1092:143–159. https://doi.org/10.1016/j.molstruc.2015.03.012
47. Sarigul M, Deveci P, Kose M. New tridentate azo–azomethines and their copper(II) complexes: Synthesis, solvent effect on tautomerism, electrochemical and biological studies. Journal of Molecular Structure. 2015;1096:64–73. https://doi.org/10.1016/j.molstruc.2015.04.043
48. Ghasemian M, Kakanejadifard A, Karami T. Spectrochimica Acta. 2016;1425:1-44.
49. Gou Y, Li J, Fan B, Xu B, Zhou M, Yang F. European Journal of Medicinal Chemistry. 2017;17:1-39.
50. Neelakantan MA, Marriappan SS, Dharmaraja J, Jeyakumar T. Spectral, XRD, SEM and biological activities of transition metal complexes of polydentate ligands containing thiazole moiety. Spectrochimica Acta Part A. 2008;71:628–635. https://doi.org/10.1016/j.saa.2008.01.023
51. Rubino S, Busà R, Attanzio A, Alduina R. Bioorganic & Medicinal Chemistry. 2017;16:1-25.
52. Abbehausen C, Sucena SF, Lancellotti M. Synthesis, spectroscopic characterization, DFT studies, and antibacterial and antitumor activities of a novel water soluble Pd(II) complex with l-alliin. Journal of Molecular Structure. 2013;1035:421–426. https://doi.org/10.1016/j.molstruc.2012.11.065
53. Ammar RA, Alaghaz A-NMA, Zayed ME, Al-Bedair LA. Journal of Molecular Structure. 2017;2860:1-42.
54. Arafath MdA, Adam F, Razali MR, Ahmed Hassan LE, Khadeer Ahamed MB, Majid AMSA. Journal of Molecular Structure. 2016;2860:1-42.
55. Rettondin AR, Carneiro ZA, Gonçalves ACR. Gold(III) complexes with ONS-Tridentate thiosemicarbazones: Toward selective trypanocidal drugs. European Journal of Medicinal Chemistry. 2016;120:217-226. https://doi.org/10.1016/j.ejmech.2016.05.003
56. Bergamoa A, Sava G. Chem. Soc. Rev. 2015;10:1-7.